

Ion acceleration from micrometric targets immersed in an intense laser field

Michal Elkind, Noam Popper, Itamar Cohen, Nitzan Alaluf, Assaf Levanon, and Ishay Pomerantz*

The School of Physics and Astronomy, Tel Aviv University, Tel Aviv, 69978, Israel and

Center for Light-Matter Interaction, Tel Aviv University, Tel Aviv, 69978, Israel

(Dated: December 20, 2024)

We report on an experimental study of proton acceleration by intense laser irradiation of micrometric bar targets, whose dimensions are transversely immersed in the laser focal volume and are longitudinally smaller than half its wavelength. With only 120 mJ of laser energy, we recorded proton energies in excess of 6 MeV, three times higher than those achieved with flat-foil irradiation using similar pulse energies. 3D particle-in-cell simulations revealed that the efficient energy transfer from the diffracted laser fields to electrons on both sides of the target, combined with its reduced surface area, results in a thicker electron sheath and higher acceleration gradients. We demonstrated numerically how this technique opens up the possibility of laser-ion acceleration in a cascaded manner, allowing manipulation of the ion spectrum by optical means.

The interaction of an intense laser pulse with matter results in the emission of multiple forms of radiation, including x-rays, electrons, ions, and positrons. This general observation has motivated three decades of research on laser-based particle acceleration. The prospect of accelerating ions on a compact scale to MeV energies and beyond has potential for many applications, including radiography of transient phenomena and strong electromagnetic fields [1], for the ion fast-ignition approach to fusion energy [2], and in generating neutron beams [3] for non-destructive testing [4]. It has particularly promising benefits in radiation therapy [5] because of the enormous cost of ion radiation therapy based on current technology, which limits the use of this treatment. A fundamental requirement for this application is the acceleration of ions to energies sufficiently high to penetrate human tissue and reach any tumor, which in the case of protons is about 250 MeV [6].

Physical mechanisms that may accelerate ions out of the bulk of an irradiated target include radiation-pressure acceleration [7], breakout afterburner [8], and collisionless shock acceleration [9]. Compared to these volumetric mechanisms on which scarce experimental data exist, target normal sheath acceleration (TNSA) [10] has been extensively studied in dozens of different experimental scenarios. TNSA relies on high-magnitude electric fields that form between an irradiated target and the electron sheath that develops around it to accelerate ions from surface contaminants. The general phenomenology is that laser systems that deliver higher pulse energies and shorter pulse durations are able to accelerate ions from flat-foil targets to higher energies [11]. For example, the current record of 150 MeV [12] has been achieved using ultrashort laser pulses with 22 J of energy, whereas 0.12 J laser pulses, like the one used for the results presented here, typically reach maximum proton energies of 2 MeV [11, 13].

In TNSA, both the lateral and longitudinal (thickness) dimensions of an irradiated target affect the characteris-

tics of the emitted ions. It is generally established that ion energies rise when the target thickness is of the order of the laser wavelength or smaller [11]. The caveat is that very thin targets would remain intact throughout the interaction to emit ions only when the laser pulse contrast is sufficiently high [14]. Limiting the transverse size of thick target foils down to 10s of micrometers was observed to enhance the accelerating gradient of the electron sheath because of electrons refluxing from the edges of the target [15–20]. But in this case, the resulting ion energies still fall short of those produced using sub-wavelength thin foils irradiated with the same laser pulse parameters [21–23].

Here we report on irradiation experiments of single formations immersed in the focal volume of an intense laser pulse and thinner than half its wavelength. These experiments resulted in proton energies higher than those achieved with any other laser-based method with a similar pulse energy. We show that this effect is not a mere combination of the two aforementioned observations about the dimensions of the target but rather a manifestation of a different and more efficient ability of the laser fields to transfer energy to the electrons that form the sheath. Hints of this dynamics could be gleaned from several experimental results showing enhanced proton emission from irradiated surfaces covered with nanometric or micrometric structures [24–27].

Irradiation of truly isolated targets fully contained within the laser focal volume is mechanically challenging and was demonstrated only by using a Paul trap to levitate single micrometer-scale plastic spheres [28, 29]. These experiments did not result in higher proton energies than those obtained with solid foils but the emitted protons featured a reduced energy bandwidth.

We studied the emission of protons from irradiated micrometric bar targets (μ -bars) made of gold. In a previous work we have shown that the interaction of an intense laser pulse with such μ -bars results in the emission of two beams of MeV-level electrons with a narrow opening angle [30]. Numeric simulations revealed that these beams consist of trains of attosecond-duration electron bunches, emitted because of the diffraction of the fields around the

* ipom@tauex.tau.ac.il

target.

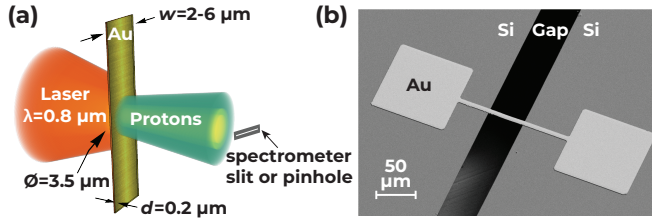


FIG. 1. The irradiation setup. (a) Illustration of the irradiation geometry. (b) SEM image of a $w = 5 \mu\text{m}$ wide μ -bar suspended over a gap in a Si substrate.

We performed the experiments using the NePTUN laser system at Tel Aviv University [31]. The irradiation geometry is illustrated in Fig. 1(a). 27-fs long (autocorrelation trace in supp. note) laser pulses of central wavelength $\lambda = 800 \text{ nm}$, with energies of 120 mJ (on-target) and pulse contrast better than 10^{11} before $t = -60 \text{ ps}$ (autocorrelation trace in supp. note) [32], that are polarized along the width (w) of the bar, were focused using an $f/2.5$ off-axis parabolic mirror unto $d = 0.2 \mu\text{m}$ thick and $w = 2 - 10 \mu\text{m}$ wide Au bar targets. 70% of the laser energy was measured to be contained within a circle of $3.5 \mu\text{m}$ diameter (see measurement in supp. note), corresponding to a normalized laser amplitude of $a_0 = 4.6$. The laser pointing stability was measured to be $0.43 \mu\text{m}$ (RMS). Spatial overlap between the target and the focused laser was achieved by imaging the target with $\times 100$ magnification under vacuum, while introducing the laser beam in low-power. A scanning electron microscope image of one such target is shown in Fig. 1(b). A detailed target fabrication procedure is given in Ref. [30] along with in situ microscope images of the laser focused on the targets.

The energy spectra of protons emitted at the laser propagation direction were measured using a Thomson parabola type ion spectrometer (TPIS) [33] operating with an electrode voltage difference of 2 kV. A charge-coupled device imaged a CsI(Tl) scintillator [34, 35] positioned at the back of the spectrometer. Absolute proton energy calibration was obtained by taking shots with parts of the scintillator covered by foil filters of known thickness and composition. The conversion of the scintillation signal to an absolute proton dose was calibrated by recording spectrometer traces using image plates [36], which were cross-calibrated using a beta emitter calibration source [13]. On a separate set of laser shots, the angular distribution of the ions were measured by placing a (0.4 mm X 25 mm) slit made of 2 mm thick Al plates, 25 mm downstream to the target. Particles passing through this aperture traversed a 0.5 T magnetic field for a distance of 25 mm, and then propagated 275 mm to a CsI(Tl) scintillating screen.

The resulting differential proton spectra for flat foils (black) and μ -bars (w in a color scale) are shown in Fig. 2(a). Each curve represents the result of a single ir-

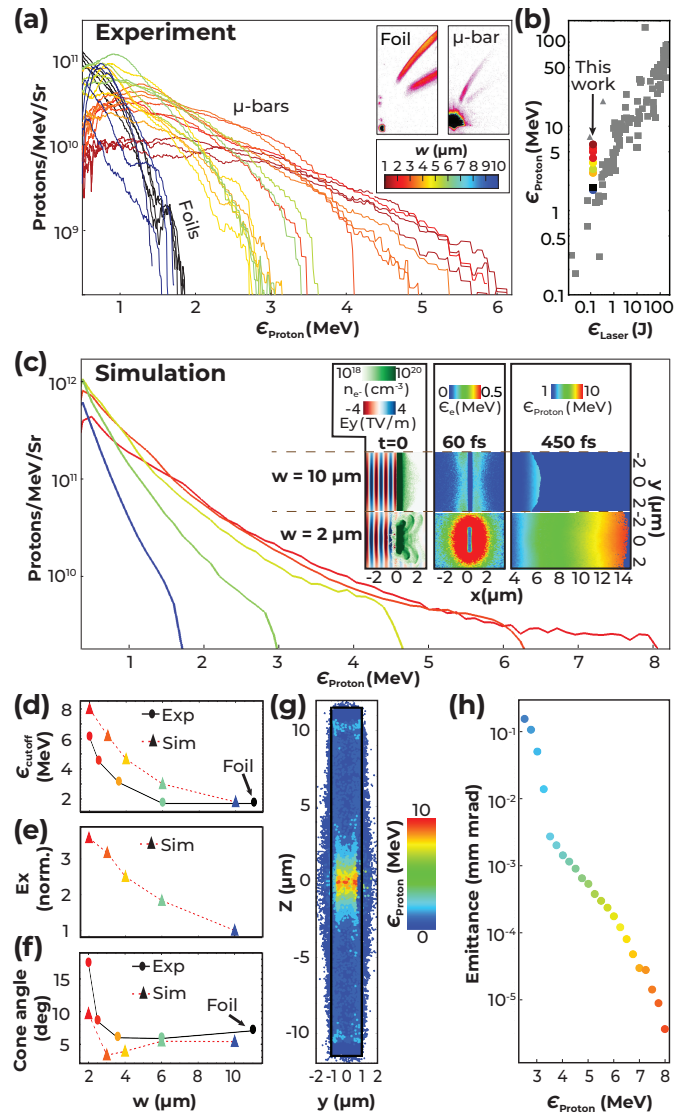


FIG. 2. The effect of the μ -bar width. (a) Experimentally measured differential proton energy spectra emitted from $d = 0.2 \mu\text{m}$ thick Au foils (black) and μ -bar targets (color scale). Example raw TPIS traces resulting from irradiation of a foil target and a $w = 1.8 \mu\text{m}$ wide μ -bar are shown as insets. (b) Compilation of the proton cutoff energies from experiments of various laser and target parameters, as a function of the laser pulse energy (gray) adapted from Ref. [11]. The results of this work are shown with the μ -bar width indicated in color. (c) Simulated differential proton energy spectra for the same experimental parameters as in (a), overlaid with snapshots of the transverse electric field (blue-to-red), electron density (green) and space averaged electron and proton energy (color scale). See supp. materials for the full simulation frames of these images. (d-f) Measured and simulated proton energy cutoffs, peak-values of the electric field in the sheath, and the cone angles of protons emitted with $E > 0.5 \text{ MeV}$ plotted vs. w . (g) Energy resolved virtual source distribution of the protons and (h) the RMS of the emittance for a $d = 0.2 \mu\text{m}$, $w = 2 \mu\text{m}$ μ -bar.

radiation experiment. Two raw spectrograms are shown

in insets for an irradiated reference 0.2 μm thick Au foil and a $d = 0.2 \mu\text{m}$ thick, $w = 1.8 \mu\text{m}$ wide μ -bar. The increased signal around the zero-point results from the electron jets that we studied in Ref. [30], impinging on the spectrometer wall. The irradiation of narrower μ -bars features higher proton cutoff energies, reaching beyond 6 MeV for $w = 2 \mu\text{m}$.

Fig. 2(b) presents a compilation of the proton cutoff energies in laser acceleration experiments as a function of the laser pulse energy, adapted from Ref. [11] and references therein. Also shown are the results of this study for the irradiation of μ -bar targets, where w is indicated with the same color scale as in Fig. 2(a). The figure shows that in a common flat-foil irradiation scenario (gray squares), a laser pulse energy higher than 1 J is required to accelerate protons to the same cutoff energies as we achieved using 120 mJ only. Also shown are results reported by Zigler et. al. (2011) [37] and Zigler et. al. (2013) [24], in which the irradiation of snow nanowires by ultrashort laser pulses of 100 mJ and 210 mJ produced proton energies of up to 7.5 MeV and 21 MeV respectively (gray triangles).

The underlying dynamics were revealed by 3D particle-in-cell (PIC) simulations using the EPOCH [38] code. In these simulations, $d = 0.2 \mu\text{m}$ thick μ -bars of various widths were irradiated with p-polarized 800-nm wavelength laser pulses having a 30 fs (FWHM) wide Gaussian temporal profile and 120 mJ of energy. The laser pulses were focused to a spot size of 3.5 μm (FWHM), yielding a normalized laser intensity of $a_0 = 4.6$. The 3D simulation space was defined as a $(32 \mu\text{m})_x \times (20 \mu\text{m})_y \times (24 \mu\text{m})_z$ box divided into $(1000)_x \times (1000)_y \times (150)_z$ computational mesh cells. We conducted one computationally heavy simulation with a high resolution of $(3000)_x \times (3000)_y \times (300)_z$ cells to verify the consistency of the results. The bulk of the targets was representative of Au^{4+} ions [39] and electrons with densities of 30 and 4×30 times that of the critical plasma density respectively. The targets were surrounded on all sides by an exponential density gradient with a scale length of $\lambda/60$. An external contaminate layer composed of H^+ , C^{4+} , and O^{4+} ions in equal parts was set with a uniform density 30 times that of the critical plasma density over a thickness of 0.1 μm [40]. The distribution of the composition of the target along the long dimension of the μ -bar was uniform over the range of $|z| < 5.5 \mu\text{m}$.

The simulation results are presented in Fig. 2(c). The differential proton energy spectra for irradiated μ -bar targets in the same parameter range as in (a) are shown with the same color scale. Overlaid are snapshots taken at $t = 0, 60,$ and 450 fs, for the cases of $w = 10 \mu\text{m}$ and $2 \mu\text{m}$ wide μ -bars. $t = 0$ represents the instant in which the peak of the laser field impinges on the μ -bar. The transverse component of the laser field (E_y) is shown in a red-to-blue color scale, with the electron density superimposed in a green color scale. The $w = 2 \mu\text{m}$ μ -bar is narrower than the laser focus and therefore is transversely immersed in the focal volume. Two trains of attosec-

ond duration electron bunches are observed to emerge with a small opening angle around the laser propagation direction. These features, which were also observed for mass-limited targets of different geometries [28, 41] were studied in detail in Ref. [30].

The experimentally observed increase in the proton cutoff energy for narrower μ -bars is captured by the simulation (Fig. 2(d)), reaching values overall higher by about 30%. Rerunning the simulations with initial ion charge states up to Au^{8+} , and with a pre-plasma scale length in the range of $\lambda/80 - \lambda/40$, resulted in an overall shift of the proton energies by a factor of 0.88–1.09, but the dependence on w remained unchanged.

Fig. 2(e) shows how the increased proton cutoff energies for narrower μ -bars are correlated with the sheath field amplitude (snapshots taken at $t = 60$ fs). The cone angles of $E > 0.5$ MeV proton beams emitted from $d = 0.2 \mu\text{m}$ μ -bar targets are plotted in Fig. 2(f) as a function of w . Both the experiment and the simulation feature a sharp increase in the divergence of the proton beam for the narrowest ($w = 2 \mu\text{m}$) targets. This geometric effect occurs when both d and w are smaller than the sheath scale length, which is on the order of microns [42], so the sheath no longer maintains the target's aspect ratio.

Energy resolved “virtual” source distributions of the proton beam [43] were obtained from the simulation results by projecting the proton angle at the end of the acceleration phase back to the target plane. These are shown in Fig. 2(g) for the case of a $d = 0.2 \mu\text{m}$, $w = 2 \mu\text{m}$ μ -bar, color-coded by the final proton energy. The normalized r.m.s. values of the proton beam emittance are shown in Fig. 2(h). These were evaluated as $(p/mc)\sigma_r\sigma_{r'}$ where $\sigma_r, \sigma_{r'}$ are the r.m.s. values of the source beam width and divergence angle [44].

So far we discussed how the lateral dimension w of the target plays a role in increasing the emitted proton energies. The effect of the target thickness d on the proton maximal energy is demonstrated in Fig. 3(a); a sharp increase of up to 15% in the proton cutoff energy (blue curve) emerge for $d < \lambda/2$ targets. This increase in energy is correlated with an increase in the peak value of the sheath electric field (red curve). Some properties of TNSA may be obtained using a simple self-similar isothermal fluid model [45, 46] in which the proton cutoff energy is given by $\epsilon_{\text{cutoff}} = 2T_e \ln[(\tau + \sqrt{\tau^2 + 1})^2]$ with $\tau = \omega_{pi} t_{\text{acc}} / \sqrt{2}e$. Here T_e is the temperature of the hot electron population, t_{acc} is an effective acceleration time, and $\omega_{pi} \sim \sqrt{n_e}$ is the ion plasma frequency. The strong dependence of ϵ_{cutoff} on T_e is observed in Fig. 3(b) where the sheath density and average electron energy were sampled at $t = 60$ fs, 1- μm behind the rear side of the target. For $d = 0.2 \mu\text{m}$ μ -bars, smaller values of w result in higher electron energies that can account for the higher energy cutoff. However, when reducing d for fixed $w = 2 \mu\text{m}$ μ -bars (Fig. 3(c)), the electron temperatures do not increase and the source of the increased proton cutoff energies is found to be the rising sheath density. To iden-

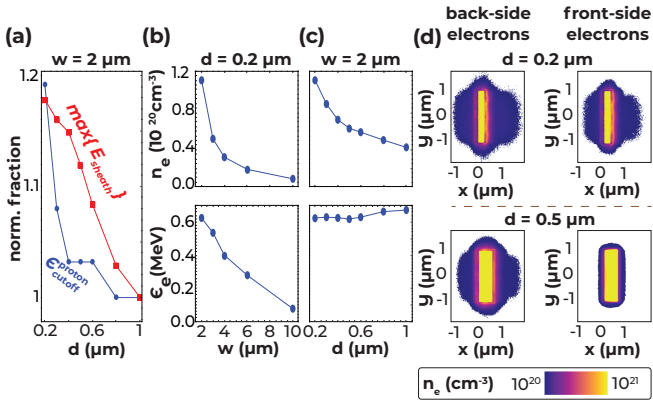


FIG. 3. The effect of the μ -bar thickness. (a) Proton cut-off energies (blue) and the maximal amplitude of the sheath field (sampled at $t = 60$ fs, red). (b) The density and average energy of electrons in the sheath sampled at $t = 60$ fs for $d = 0.2$ μm and $w = 2$ – 10 μm μ -bars. (c) Same as (b) for $w = 2$ μm and $d = 0.2$ – 1.0 μm μ -bars. (d) Density distributions of the electron sheath forming at $t = 60$ fs around $w = 2$ μm , $d = 0.2$ μm (top) and 0.5 μm (bottom) μ -bars. Electrons originating from the front side or the back side of the target are shown on the left and right respectively.

tify the origin of this thicker sheath, we separated the electron population according to the surface from which they originated. Fig. 3(d) presents sheath density distributions forming around $w = 2$ μm μ -bars at $t = 60$ fs. Electrons that initially covered the plasma gradient at the front ($x < 0$) of the target are shown on the left, and those that originated from the back side ($x - d > 0$) are shown on the right. For a target thinner than half the laser wavelength (top, $d = 0.2$ μm), the sheath is a mixture of front and back electrons. However, when the μ -bar is thicker than half the laser wavelength (bottom, $d = 0.5$ μm), the sheath is observed to consist of front-side electrons only.

The use of micrometric formations as targets for TNSA of ions suggests the possibility of cascaded ion acceleration by sequential irradiation of multiple targets. This method has been attempted using solid foils [47, 48], but because the numerical aperture in this irradiation scenario is on the order of unity, the separation distance between the two targets must be kept close to their lateral dimension to allow a second laser pulse to fit between the targets. Indeed, the separation between the foil targets in those experiments was on the order of millimeters, resulting in a dispersed proton bunch that is much larger than the sheath of the second target, thus making the secondary acceleration inefficient.

We demonstrate numerically the potential of a cascaded proton accelerator composed of micrometric targets in Fig. 4. Two $d = 0.2$ μm μ -bars are positioned parallel to their $w = 2$ μm sides, with a separation of 6 μm between them. The targets are irradiated at a 45° angle of incidence with two laser pulses, having the same parameters as in the simulations presented in Fig. 3, with

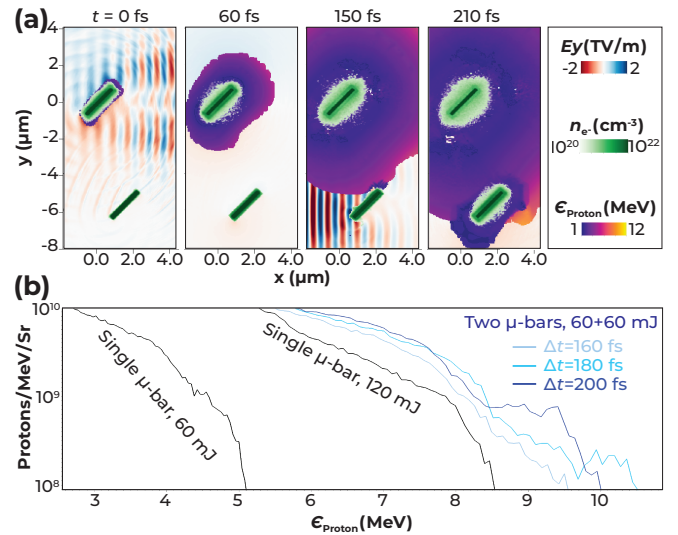


FIG. 4. 3D PIC simulation of a cascaded proton accelerator based on the irradiation of two μ -bars. Each μ -bar was irradiated with a 25 fs long, 60 mJ laser pulse at a 45° angle of incidence. The second pulse follows the first one with a $\Delta t = 180$ fs delay. (a) Snapshots of the transverse component of the electric field (E_y) are shown in a red-to-blue color scale, with the electron density overlaid in green and the space-averaged energy of protons in a color scale. At $t = 210$ fs, protons that were emitted from the first μ -bar are observed to be further accelerated by the sheath of the second μ -bar to energies above 10 MeV. (b) The resulting differential proton energy spectra from the simulation shown in (a), compared to simulations with shorter ($\Delta t = 160$) or longer ($\Delta t = 200$) delays between the two pulses. The spectra are also compared with those resulting from the irradiation of a single μ -bar with a 25 fs long laser pulse of 60 or 120 mJ.

the laser energy distributed evenly between them. The second pulse is delayed by $\Delta t = 180$ fs with respect to the first, so an electron sheath forms around the second μ -bar at the time of arrival of ~ 4 MeV protons emitted from the first target. The position of the second μ -bar is chosen at the minimal separation in which the intensity of the first pulse would not induce a sheath around it prematurely, taking advantage of the increased divergence of the proton beam discussed above. Fig. 4(a) shows four snapshots of the transverse component of the laser field (red-to-blue), electron density (green), and the space-averaged proton energy (color scale). The final snapshot demonstrates how the sheath around the second target further accelerates those protons to energies of over 10 MeV. The resulting differential energy spectra of the emitted protons is shown in Fig. 4(b). It is also compared to two identical simulations in which the second pulse arrive too early ($\Delta t = 160$ fs) or too late ($\Delta t = 200$ fs), resulting in lower proton cut-off energies.

In comparison to the double-foil target experiments discussed above, we may consider for example a beam of protons emitted from the first target with energies close to 5 MeV, and a 1 μm thick sheath prevailing for 50 fs

of effective acceleration time [46] around the second target. A 6- μm separation distance will correspond to effective acceleration of 5 ± 0.64 MeV protons, while a 1-mm separation distance will only accelerate protons arriving within 5 ± 0.004 MeV.

Compared to the common irradiation scenario of flat foil targets, the widest $\mu\text{-bar}$ targets we irradiated ($w = 6 \mu\text{m}$), produce the same absolute spectrum of protons above $E > 1.5$ MeV (Fig. 2(a)). For narrower targets, the total number of protons roughly scale linearly with w which implies scaling with the target's surface area. Going from a foil target to the narrowest $\mu\text{-bar}$ of $w = 2 \mu\text{m}$, we observe a drop of 32% in the conversion efficiency from the laser pulse energy to the total energy of the emitted protons. The measured differential proton flux and the conversion efficiency of the laser pulse energy to the proton beam are presented in Supp. note.

Few practical aspects in the irradiation of $\mu\text{-bar}$ targets should be considered. First, unlike planar targets which are transversely larger than the focus dimensions, $\mu\text{-bars}$ are more susceptible to intensity drops resulting from the pointing instability on the laser system. Second, while proton production targets in the form of massive rotating disks [49], spooled tape [50], and jets of liquids, gasses, and molecular clusters [51–54] demonstrated target replenishment with Hz – kHz rates, systems designed to deliver micromachined targets mounted on either whole wafers [13] or small chips [55] operate at sub-Hz rates only and their ability to position targets with sub-micrometer accuracy in the transverse direction is yet to be demonstrated. Finally, understanding the sensitivity of the acceleration to the intensity of precursor light is paramount to evaluating the scalability of our findings to larger laser systems. This future study will be conducted through time-resolved plasma interferometry of the target's pre-expansion.

An additional strong-suit of using $\mu\text{-bar}$ targets for TNSA is the small 'virtual' source size [43] of the protons. This property sets a limit on the spatial resolution when performing proton radiography, a method used for a wide range of basic research [1] and medical applica-

tions [56]. In TNSA off planar foils the virtual source size is of the order of 10 μm [43, 57, 58], while for a $\mu\text{-bar}$ (Fig. 2(g)) it is found to be smaller than 1 μm for the high energy part of the proton beam. This advantage is further highlighted by the low transverse emittance of the proton beam plotted in Fig. 2(h), which drops well below the values typical to planar foil targets of about 10^{-3} mm mrad [44].

In summary, we discovered that the interaction of an intense laser pulse with an object whose dimensions are transversely immersed in the focal volume and thinner than half the laser wavelength results in enhanced TNSA, with the emitted protons reaching 3 times the energy of those obtained with a conventional planar foil target. By irradiating 2 μm wide, 0.2 μm thick gold bar targets we accelerated protons to over 6 MeV using only 120 mJ of laser energy on-target. We note that for the acceleration of ions heavier than H^+ , other methods such as the Coloumb explosion of molecular clusters [54] were able to generate even higher ion energies using the same laser pulse energy.

Beyond the increase in ion energies, the smaller target dimensions provide a small virtual source size and low emittance, and make possible cascaded acceleration by irradiation of multiple targets with micrometric spacing, which could provide even higher proton energies and optical means to control their spectrum.

ACKNOWLEDGMENTS

This research was supported by Israel Science Foundation Grant No. 2314/21. We acknowledge the aid in the fabrication of the targets from the Tel Aviv University Center for Nanoscience and Nanotechnology. Simulations were performed using EPOCH, which was developed as part of the UK Engineering and Physical Sciences Research Council (EPSRC)-funded Project No. EP/G054940/1. I.P. acknowledges the support of the Zuckerman STEM Leadership Program.

-
- [1] D. B. Schaeffer, A. F. A. Bott, M. Borghesi, K. A. Flippo, W. Fox, J. Fuchs, C. Li, F. H. Séguin, H.-S. Park, P. Tzeferacos, and L. Willingale, Proton imaging of high-energy-density laboratory plasmas, *Rev. Mod. Phys.* **95**, 045007 (2023).
 - [2] J. Fernández, B. Albright, F. N. Beg, M. E. Foord, B. M. Hegelich, J. Honrubia, M. Roth, R. B. Stephens, and L. Yin, Fast ignition with laser-driven proton and ion beams, *Nuclear fusion* **54**, 054006 (2014).
 - [3] M. Roth, D. Jung, K. Falk, N. Guler, O. Deppert, M. Devlin, A. Favalli, J. Fernandez, D. Gautier, M. Geissel, *et al.*, Bright laser-driven neutron source based on the relativistic transparency of solids, *Physical review letters* **110**, 044802 (2013).
 - [4] I. Kishon, A. Kleinschmidt, V. Schanz, A. Tebartz, O. Noam, J. Fernandez, D. Gautier, R. Johnson, T. Shimada, G. Wurden, *et al.*, Laser based neutron spectroscopy, *Nuclear Instruments and Methods in Physics Research Section A: Accelerators, Spectrometers, Detectors and Associated Equipment* **932**, 27 (2019).
 - [5] K. W. Ledingham, P. R. Bolton, N. Shikazono, and C.-M. C. Ma, Towards laser driven hadron cancer radiotherapy: A review of progress, *Applied Sciences* **4**, 402 (2014).
 - [6] H. Kumada, Accelerator systems for proton radiotherapy, *Proton Beam Radiotherapy: Physics and Biology*, 85 (2020).
 - [7] A. Henig, S. Steinke, M. Schnürer, T. Sokollik, R. Hörlein, D. Kiefer, D. Jung, J. Schreiber, B. Hegelich, X. Yan, *et al.*, Radiation-pressure acceleration of ion

- beams driven by circularly polarized laser pulses, *Physical Review Letters* **103**, 245003 (2009).
- [8] B. Hegelich, I. Pomerantz, L. Yin, H. Wu, B. Albright, D. Gautier, S. Letzring, S. Palaniyappan, R. Shah, *et al.*, Laser-driven ion acceleration from relativistically transparent nanotargets, *New Journal of Physics* **15**, 085015 (2013).
- [9] L. O. Silva, M. Marti, J. R. Davies, R. A. Fonseca, C. Ren, F. S. Tsung, and W. B. Mori, Proton shock acceleration in laser-plasma interactions, *Physical Review Letters* **92**, 015002 (2004).
- [10] M. Passoni, L. Bertagna, and A. Zani, Target normal sheath acceleration: theory, comparison with experiments and future perspectives, *New Journal of Physics* **12**, 045012 (2010).
- [11] M. Zimmer, S. Scheuren, T. Ebert, G. Schaumann, B. Schmitz, J. Hornung, V. Bagnoud, C. Rödel, and M. Roth, Analysis of laser-proton acceleration experiments for development of empirical scaling laws, *Physical Review E* **104**, 045210 (2021).
- [12] T. Ziegler, I. Göthel, S. Assenbaum, C. Bernert, F.-E. Brack, T. E. Cowan, N. P. Dover, L. Gaus, T. Kluge, S. Kraft, *et al.*, Laser-driven high-energy proton beams from cascaded acceleration regimes, *Nature Physics* , 1 (2024).
- [13] Y. Gershuni, D. Roitman, I. Cohen, E. Porat, Y. Danan, M. Elkind, A. Levanon, R. Louzon, D. Reichenberg, A. Tsabary, *et al.*, A gatling-gun target delivery system for high-intensity laser irradiation experiments, *Nuclear Instruments and Methods in Physics Research Section A: Accelerators, Spectrometers, Detectors and Associated Equipment* **934**, 58 (2019).
- [14] S. Keppler, N. Elkina, G. Becker, J. Hein, M. Hornung, M. Mäusezahl, C. Rödel, I. Tamer, M. Zepf, and M. Kaluza, Intensity scaling limitations of laser-driven proton acceleration in the tnsa-regime, *Physical Review Research* **4**, 013065 (2022).
- [15] S. Buffechoux, J. Psikal, M. Nakatsutsumi, L. Romagnani, A. Andreev, K. Zeil, M. Amin, P. Antici, T. Burris-Mog, A. Compant-La-Fontaine, *et al.*, Hot electrons transverse refluxing in ultraintense laser-solid interactions, *Physical review letters* **105**, 015005 (2010).
- [16] S. D. Kraft, L. Obst, J. Metzkes-Ng, H.-P. Schlenvoigt, K. Zeil, S. Michaux, D. Chatain, J.-P. Perin, S. N. Chen, J. Fuchs, *et al.*, First demonstration of multi-mev proton acceleration from a cryogenic hydrogen ribbon target, *Plasma Physics and Controlled Fusion* **60**, 044010 (2018).
- [17] K. Zeil, J. Metzkes, T. Kluge, M. Bussmann, T. Cowan, S. Kraft, R. Sauerbrey, B. Schmidt, M. Zier, and U. Schramm, Robust energy enhancement of ultrashort pulse laser accelerated protons from reduced mass targets, *Plasma Physics and Controlled Fusion* **56**, 084004 (2014).
- [18] T. Toncian, M. Swantusch, M. Toncian, O. Willi, A. Andreev, and K. Platonov, Optimal proton acceleration from lateral limited foil sections and different laser pulse durations at relativistic intensity, *Physics of Plasmas* **18** (2011).
- [19] O. Tresca, D. Carroll, X. Yuan, B. Aurand, V. Bagnoud, C. Brenner, M. Coury, J. Fils, R. Gray, T. Kühl, *et al.*, Controlling the properties of ultraintense laser-proton sources using transverse refluxing of hot electrons in shaped mass-limited targets, *Plasma physics and controlled fusion* **53**, 105008 (2011).
- [20] Y. Fang, X. Ge, S. Yang, W. Wei, T. Yu, F. Liu, M. Chen, J. Liu, X. Yuan, Z. Sheng, *et al.*, Different effects of laser contrast on proton emission from normal large foils and transverse-size-reduced targets, *Plasma Physics and Controlled Fusion* **58**, 075010 (2016).
- [21] J. Green, A. Robinson, N. Booth, D. Carroll, R. Dance, R. Gray, D. MacLellan, P. McKenna, C. Murphy, D. Rusby, *et al.*, High efficiency proton beam generation through target thickness control in femtosecond laser-plasma interactions, *Applied Physics Letters* **104** (2014).
- [22] J. Hornung, Y. Zobus, P. Boller, C. Brabetz, U. Eisenbarth, T. Kühl, Z. Major, J. Ohland, M. Zepf, B. Zielbauer, *et al.*, Enhancement of the laser-driven proton source at phelix, *High Power Laser Science and Engineering* **8**, e24 (2020).
- [23] S. Busold, *Construction and characterization of a laser-driven proton beamline at GSI*, Ph.D. thesis (2014).
- [24] A. Zigler, S. Eisenman, M. Botton, E. Nahum, E. Schleifer, A. Baspaly, I. Pomerantz, F. Abicht, J. Branzel, G. Priebe, S. Steinke, A. Andreev, M. Schnuerer, W. Sandner, D. Gordon, P. Sprangle, and K. W. D. Ledingham, Enhanced Proton Acceleration by an Ultrashort Laser Interaction with Structured Dynamic Plasma Targets, *Physical review letters* **110**, 215004 (2013).
- [25] V. Floquet, O. Klimo, J. Psikal, A. Velyhan, J. Limpouch, J. Proska, F. Novotny, L. Stolcova, A. Macchi, A. Sgattoni, L. Vassura, L. Labate, F. Baffigi, L. A. Gizzi, P. Martin, and T. Ceccotti, Micro-sphere layered targets efficiency in laser driven proton acceleration, *J. Appl. Phys* **114**, 83305 (2013).
- [26] D. Margarone, O. Klimo, I. Kim, J. Prokupek, J. Limpouch, T. Jeong, T. Mocek, J. Psikal, H. Kim, J. Proska, *et al.*, Laser-driven proton acceleration enhancement by nanostructured foils, *Physical review letters* **109**, 234801 (2012).
- [27] A. Curtis, C. Calvi, J. Tinsley, R. Hollinger, V. Kaymak, A. Pukhov, S. Wang, A. Rockwood, Y. Wang, V. N. Shlyaptsev, *et al.*, Micro-scale fusion in dense relativistic nanowire array plasmas, *Nature communications* **9**, 1077 (2018).
- [28] T. M. Ostermayr, D. Haffa, P. Hilz, V. Pauw, K. Allinger, K.-U. Bamberg, P. Böhl, C. Bömer, P. R. Bolton, F. Deutschmann, T. Ditmire, M. E. Donovan, G. Dyer, E. Gaul, J. Gordon, B. M. Hegelich, D. Kiefer, C. Klier, C. Kreuzer, M. Martinez, E. McCary, A. R. Meadows, N. Moschüring, T. Rösch, H. Ruhl, M. Spinks, C. Wagner, and J. Schreiber, Proton acceleration by irradiation of isolated spheres with an intense laser pulse, *Phys. Rev. E* **94**, 033208 (2016).
- [29] P. Hilz, T. Ostermayr, A. Huebl, V. Bagnoud, B. Borm, M. Bussmann, M. Gallei, J. Gebhard, D. Haffa, J. Hartmann, *et al.*, Isolated proton bunch acceleration by a petawatt laser pulse, *Nature communications* **9**, 423 (2018).
- [30] M. Elkind, I. Cohen, D. Blackman, T. Meir, L. Perlmutter, T. Catabi, A. Levanon, S. H. Glenzer, A. V. Arefiev, and I. Pomerantz, Intense laser interaction with microbars, *Scientific Reports* **13**, 21345 (2023).
- [31] E. Porat, A. Levanon, D. Roitman, I. Cohen, R. Louzon, and I. Pomerantz, Towards direct-laser-production of relativistic surface harmonics, in *Relativistic Plasma Waves and Particle Beams as Coherent and Incoherent Radia-*

- tion Sources III*, Vol. 11036 (SPIE, 2019) pp. 35–40.
- [32] E. Porat, H. Yehuda, I. Cohen, A. Levanon, and I. Pomerantz, Diffraction-limited coherent wake emission, *Phys. Rev. Research* **3**, L032059 (2021).
- [33] J. Morrison, C. Willis, R. Freeman, and L. Van Woerkom, Design of and data reduction from compact thomson parabola spectrometers, *Review of Scientific Instruments* **82** (2011).
- [34] A. Pappalardo, L. Cosentino, and P. Finocchiaro, An imaging technique for detection and absolute calibration of scintillation light, *Review of Scientific Instruments* **81**, 10.1063/1.3360931 (2010).
- [35] I. Cohen, T. Meir, K. Tangtharakul, L. Perelmutter, M. Elkind, Y. Gershuni, A. Levanon, A. V. Arefiev, and I. Pomerantz, Undepleted direct laser acceleration, *Science Advances* **10**, eadk1947 (2024).
- [36] A. Mančić, J. Fuchs, P. Antici, S. Gaillard, and P. Audebert, Absolute calibration of photostimulable image plate detectors used as (0.5–20mev) high-energy proton detectors, *Review of Scientific Instruments* **79** (2008).
- [37] A. Zigler, T. Palchan, N. Bruner, E. Schleifer, S. Eisenmann, M. Botton, Z. Henis, S. A. Pikuz, A. Y. Faenov, D. Gordon, and P. Sprangle, 5.5–7.5 mev proton generation by a moderate-intensity ultrashort-pulse laser interaction with h₂O nanowire targets, *Phys. Rev. Lett.* **106**, 134801 (2011).
- [38] T. Arber, K. Bennett, C. Brady, A. Lawrence-Douglas, M. Ramsay, N. Sircombe, P. Gillies, R. Evans, H. Schmitz, A. Bell, *et al.*, Contemporary particle-in-cell approach to laser-plasma modelling, *Plasma Physics and Controlled Fusion* **57**, 113001 (2015).
- [39] D. Kawahito and Y. Kishimoto, Ionization and acceleration of multiply charged gold ions in solid film irradiated by high intensity laser, *Physics of Plasmas* **27** (2020).
- [40] T. Kluge, W. Enghardt, S. D. Kraft, U. Schramm, K. Zeil, T. E. Cowan, and M. Bussmann, Enhanced laser ion acceleration from mass-limited foils, *Physics of Plasmas* **17**, 123103 (2010).
- [41] D. E. Cardenas, T. M. Ostermayr, L. Di Lucchio, L. Hofmann, M. F. Kling, P. Gibbon, J. Schreiber, and L. Veisz, Sub-cycle dynamics in relativistic nanoplasma acceleration, *Scientific Reports* 2019 9:1 **9**, 1 (2019).
- [42] O. Jäckel, J. Polz, S. Pfoth, H. Schlenvoigt, H. Schwoerer, and M. Kaluza, All-optical measurement of the hot electron sheath driving laser ion acceleration from thin foils, *New Journal of Physics* **12**, 103027 (2010).
- [43] M. Borghesi, A. Mackinnon, D. H. Campbell, D. Hicks, S. Kar, P. K. Patel, D. Price, L. Romagnani, A. Schiavi, and O. Willi, Multi-mev proton source investigations in ultraintense laser-foil interactions, *Physical Review Letters* **92**, 055003 (2004).
- [44] M. Roth and M. Schollmeier, Ion acceleration-target normal sheath acceleration, arXiv preprint arXiv:1705.10569 (2017).
- [45] P. Mora, Plasma expansion into a vacuum, *Physical Review Letters* **90**, 185002 (2003).
- [46] J. Fuchs, P. Antici, E. d’Humières, E. Lefebvre, M. Borghesi, E. Brambrink, C. Cecchetti, M. Kaluza, V. Malka, M. Manclossi, *et al.*, Laser-driven proton scaling laws and new paths towards energy increase, *Nature physics* **2**, 48 (2006).
- [47] S. Pfoth, O. Jäckel, J. Polz, S. Steinke, H. Schlenvoigt, J. Heymann, A. Robinson, and M. Kaluza, A cascaded laser acceleration scheme for the generation of spectrally controlled proton beams, *New Journal of Physics* **12**, 103009 (2010).
- [48] W. Wang, B. Shen, H. Zhang, X. Lu, J. Li, S. Zhai, S. Li, X. Wang, R. Xu, C. Wang, *et al.*, Multi-stage proton acceleration controlled by double beam image technique, *Physics of Plasmas* **25** (2018).
- [49] B. Hou, J. Nees, J. Easter, J. Davis, G. Petrov, A. Thomas, and K. Krushelnick, Mev proton beams generated by 3 mj ultrafast laser pulses at 0.5 khz, *Applied Physics Letters* **95** (2009).
- [50] M. Noaman-ul Haq, H. Ahmed, T. Sokollik, L. Yu, Z. Liu, X. Yuan, F. Yuan, M. Mirzaie, X. Ge, L. Chen, *et al.*, Statistical analysis of laser driven protons using a high-repetition-rate tape drive target system, *Physical Review Accelerators and Beams* **20**, 041301 (2017).
- [51] J. T. Morrison, S. Feister, K. D. Frische, D. R. Austin, G. K. Ngirmang, N. R. Murphy, C. Orban, E. A. Chowdhury, and W. Roquemore, Mev proton acceleration at khz repetition rate from ultra-intense laser liquid interaction, *New Journal of Physics* **20**, 022001 (2018).
- [52] H.-G. Chou *et al.*, High-repetition-rate, multi-mev deuteron acceleration from converging heavy water microjets at laser intensities of 1021 w/cm², *Applied Physics Letters* **121** (2022).
- [53] L. Willingale, S. Mangles, P. Nilson, R. Clarke, A. Dangor, M. Kaluza, S. Karsch, K. Lancaster, W. Mori, Z. Najmudin, *et al.*, Collimated multi-mev ion beams from high-intensity laser interactions? format?¿ with underdense plasma, *Physical review letters* **96**, 245002 (2006).
- [54] Y. Fukuda, A. Y. Faenov, M. Tampo, T. Pikuz, T. Nakamura, M. Kando, Y. Hayashi, A. Yogo, H. Sakaki, T. Kameshima, *et al.*, Energy increase in multi-mev ion acceleration in the interaction of a short pulse laser with a cluster-gas target, *Physical review letters* **103**, 165002 (2009).
- [55] I. Cohen, T. Cohen, A. Levinson, M. Elkind, Y. Rakovsky, A. Levanon, D. Michaeli, E. Cohen, A. Beck, and I. Pomerantz, Accumulated laser-photon-neutron generation, *The European Physical Journal Plus* **139**, 1 (2024).
- [56] R. P. Johnson, Review of medical radiography and tomography with proton beams, *Reports on progress in physics* **81**, 016701 (2017).
- [57] W. Wang, B. Shen, H. Zhang, X. Lu, C. Wang, Y. Liu, L. Yu, Y. Chu, Y. Li, T. Xu, *et al.*, Large-scale proton radiography with micrometer spatial resolution using femtosecond petawatt laser system, *AIP Advances* **5** (2015).
- [58] D. Li, X. Xu, T. Yang, M. Wu, Y. Zhang, H. Cheng, X. Hu, Y. Geng, J. Zhu, Y. Zhao, *et al.*, Influence factors of resolution in laser accelerated proton radiography and image deblurring, *AIP Advances* **11** (2021).